JACS
JOURNAL OF THE AMERICAN CHEMICAL SOCIETY

ARTICLE

pubs.acs.org/JACS

Robust Control of Microdomain Orientation in Thin Films of Block Copolymers by Zone Casting

Chuanbing Tang,[*,†] Wei Wu,[‡] Detlef-M. Smilgies,[§] Krzysztof Matyjaszewski,[*,‡] and Tomasz Kowalewski[*,‡]

[†]Department of Chemistry and Biochemistry and Nanocenter, University of South Carolina, Columbia, 631 Sumter Street, Columbia, South Carolina 29208, United States

[‡]Department of Chemistry, Carnegie Mellon University, 4400 Fifth Avenue, Pittsburgh, Pennsylvania 15213, United States

[§]Cornell University, CHESS, Ithaca, New York 14853, United States

Supporting Information

ABSTRACT: Block copolymers with chemically immiscible segments exhibit a variety of microphase-separated nanostructures on the scale of 10−100 nm. Controlling the orientation of these microphase separated nanostructures is vital in many applications such as lithography, membranes, data storage, and so forth. Typical strategies involve the use of external fields or patterned substrates. Here, we report a robust zone casting technique to achieve highly ordered thin films of block copolymers on centimeter-scale substrates. The robustness of this technique is its powerful control on diverse morphologies and exceptional tolerance on versatility of block copolymer chemistry as well as allowance of a wide spectrum of substrates. We demonstrate that perpendicular orientations with respect to the surface are achieved for block copolymers with both lamellar and cylindrical morphologies by controlling solution casting rate, temperatures, and block copolymer chemical structures. Thin films of both noncrystalline and crystalline block copolymers exhibit excellent orientational order and lateral order. However, the lateral order in the thin films of crystalline block copolymers shows dependence on casting temperature and melting temperature of the crystalline segment. Remarkably, all the ordering is independent of the substrates on which the block copolymer films are cast.

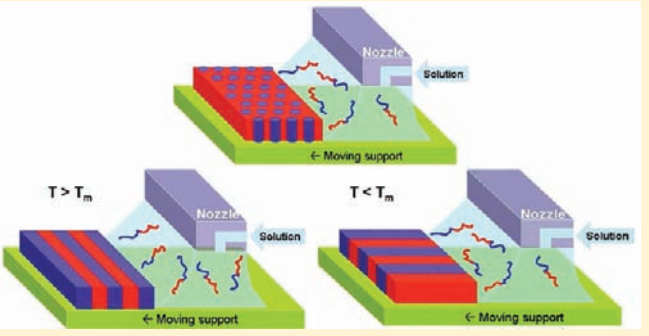

INTRODUCTION

Self-assembly of small molecules and macromolecules has attracted significant interests due to the potential to guide the fabrication of electronic devices on the order of tens of nanometers.[1−3] Block copolymers with chemically immiscible segments present as one of the most promising candidates for fabrication of many modern microelectronics, as they can phase separate into a variety of nanostructures, such as spheres, cylinders, gyroids, and lamellae, on the scale of 10−100 nm.[4−15] For many applications in thin films such as membranes, data storage, masks for lithography, and so forth,[16−19] it is generally desirable that cylinders and lamellae of block copolymers are aligned perpendicular to the surface with long-range orientational and lateral order.[20−23] However, for a diblock copolymer (with blocks A and B), a random parallel orientation of cylinders and lamellae with respect to the surface is often observed given that the difference of their interfacial energies ($\Delta\gamma = \gamma_A - \gamma_B$) is usually large.[21,22,24] A neutral surface (where $\gamma_A \approx \gamma_B$) would lead to a perpendicular orientation. One of the possible ways to achieve such orientation is to introduce random copolymers of A and B as a brush layer to tune the surface energy,[24,25] even though such nanostructures often lack long-range order, and the typical grain size over which the block copolymer domains are ordered is in the submicrometer range. Known strategies to prepare highly ordered block copolymer films include the use of external force such as electrical field[26−30] magnetic field,[31] shear force,[32] confined surfaces such as graphoepitaxy[33−39] and chemically patterned substrate,[17,40] directional solidification,[41,42] and solvent annealing.[43−51] Recently, highly ordered thin films of a diblock copolymer could be achieved by controlling the interface through droplet pinning on a tilted surface.[52] However, most of current technologies do not have the ability to achieve long-range order with diverse morphologies and to allow versatile block copolymers on a variety of substrates.

Herein, we report the use of a robust unidirectional solution casting method, known as zone casting, to prepare highly ordered block copolymer films with diverse morphologies on numerous centimeter-scale substrates. We demonstrate the potential that this technique could be generalized to prepare a variety of block copolymers with different physical properties including noncrystalline and crystalline block copolymers. Zone casting was originally designed to orient small crystalline molecules such as hexabenzocoronene.[47,53,54] Our early studies showed that it can

Received: May 23, 2011
Published: June 27, 2011

Scheme 1. A Zone Casting Technique toward Highly Ordered Perpendicular Cylinders (A) and Lamellae (B) of Noncrystalline Block Copolymer Thin Films

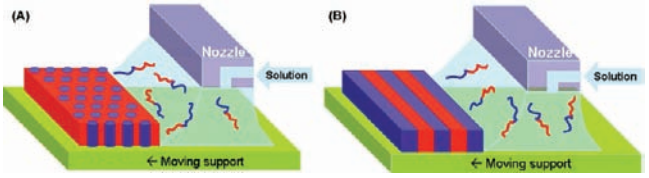

be used to prepare highly ordered lamellar polyacrylonitrile-*b*-poly(*n*-butyl acrylate) (PAN-*b*-P*n*BA) block copolymers, which were subsequently converted into ordered carbon.[55] In zone casting, as shown in Scheme 1, a polymer solution is injected through a nozzle via a computer-controlled syringe pump and spreads along a Teflon rod through capillary force. The polymer solution along the Teflon rod produces a meniscus on a substrate only less than 1 mm underneath, which moves along a parallel direction to the solution injection. The polymers would solidify along the solid−liquid interface (solidification front), near where there is a concentration gradient of polymer solution and rapid solvent evaporation. Both the solution casting (injection) rate and substrate withdrawal rate are controlled to allow the polymer solidification and solvent evaporation to reach equilibrium. Temperatures of both the polymer solution and the substrate are adjusted to achieve an appropriate solvent evaporation rate. The thickness of films can be controlled by adjusting the substrate withdrawal rate and the polymer concentration, ranging from below 100 nm to a few micrometers. Our earlier study indicated that proper control of the interface along the solidification front allowed us to prepare highly ordered thin films of a noncrystalline PAN-*b*-P*n*BA block copolymer with a lamellar morphology.[55] The key of this technique is to define the ordered domain nucleation at the solidification front and to control its advancing rate through the solution evaporation.

In this paper, we first explored a noncrystalline block copolymer system of polystyrene-*b*-polybutadiene (PS-*b*-PB) with a cylindrical morphology. We were able to produce highly ordered thin films with the cylinders perpendicular to the surface. The PB domains formed ordered single grains, the size of which primarily depended on the substrate withdrawal rate. In a semicrystalline system of poly(octadecyl methacrylate)-*b*-poly(*t*-butyl acrylate)-*b*-poly(octadecyl methacrylate) (PODMA-*b*-P*t*BA-*b*-PODMA), the lamellae were perpendicular to the substrate. However, in the lateral plane, the orientation of the lamellae was observed to be significantly affected by the casting temperature. In particular, we demonstrated how the orientation of block copolymer lamellae was affected by the interplay between the crystallization and microphase separation at the solidification front.

RESULTS AND DISCUSSION

Thin Films of Cylindrical Block Copolymers by Zone-Casting. The PS-*b*-PB block copolymers dissolved in chloroform with a concentration of 10 mg/mL was zone cast on a variety of substrates. A Tapping Mode Atomic Force Microscopy (TMAFM) height image (Figure 1A) of the PS-*b*-PB block copolymer film on a silicon wafer with the substrate withdrawal rate at 18 μm/s showed ordered arrays of circular depressions (softer PB) within the more rigid matrix (PS). The corresponding phase contrast image of films (Figure 1B) exhibited a characteristic morphology

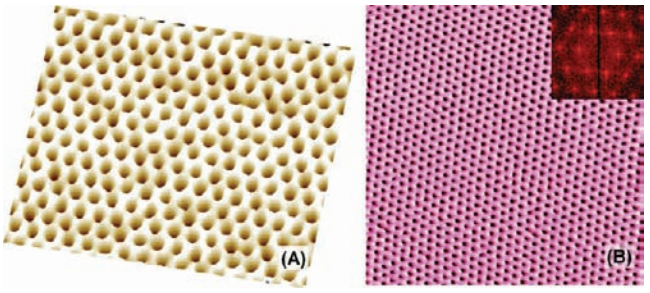

Figure 1. TMAFM images of a single grain of thin films of PS-*b*-PB block copolymers prepared by zone casting on a silicon wafer with the substrate withdrawal speed at 18 μm/s: (A) height image (500 nm × 500 nm); (B) phase image (1.0 μm × 1.0 μm). Inset: FT spectrum. Film thickness = ~1000 nm.

with mechanically weaker cylindrical PB cylinders (darker features) oriented perpendicular to the film surface and hexagonally packed within the PS matrix. The lattice spacing of this hexagonal texture was determined by 2-D Fourier transform (FT) of AFM images and was equal to 30.6 nm, which was very close to the 31 nm spacing in analogous bulk materials of the same block copolymer determined by Russell group using small-angle X-ray scattering (SAXS).[52] The images and the associated FT clearly showed that the displayed 1 μm × 1 μm area consisted of a single grain of hexagonally packed ordered PB cylinders. Random inspection of other regions revealed that the orientational order of perpendicular PB cylinders extended over the entire sample area (3 cm × 5 cm). Similar patterns were obtained on several different substrates such as carbon-coated silicon wafer, mica, carbon-coated mica, Kapton (aromatic polyimide), and quartz. It is interesting to note that another directional casting technique induced ordering of the same block copolymer with the PB cylinders parallel to the surface.[52]

Remarkably, the ordered grain size exhibited a strong dependence on the substrate withdrawal rate. For samples prepared with a withdrawal rate as low as 2 μm/s, single grains extended over the distance as large as 10 μm (Figure 2A and Supporting Information Figure S1), in both directions parallel and perpendicular to the substrate withdrawal direction. With the increase of the substrate withdrawal rate, the grain size decreased dramatically (Figure S4). For samples cast at 500 μm/s, the grain size was smaller than 100 nm (Figure 2D) and the FT pattern was nearly circular. Both perpendicular and parallel cylinders were observed. The morphologies resembled those samples prepared by spin-coating and subsequent thermal annealing.[52] For samples cast at the rate of 6 and 102 μm/s, the grain sizes were up to 5.5 and 1.5 μm, respectively (Figures S2 and S3). The film thickness decreased monotonically with the increase of casting speed.

TEM analysis of OsO_4-stained cross sections of zone-cast films revealed that the orientation of the PB cylinders normal to the film surface extended to a certain depth toward the substrate, with the depth increasing with the decrease of the substrate withdrawal rate (Figure 3). In contrast, for the withdrawal rate at 102 μm/s, the penetration depth of perpendicular cylinders was only on the order of 50 nm (Figure 3F). The depth increased to about 1 μm for films obtained at the casting rate of 2 μm/s (Figure 3A). Interestingly, the penetration depth of cylinders increased monotonically with the increase of ordered grain size. Given this observation, larger grain size and deeper penetration of perpendicular cylinders can be achieved by further reducing the substrate

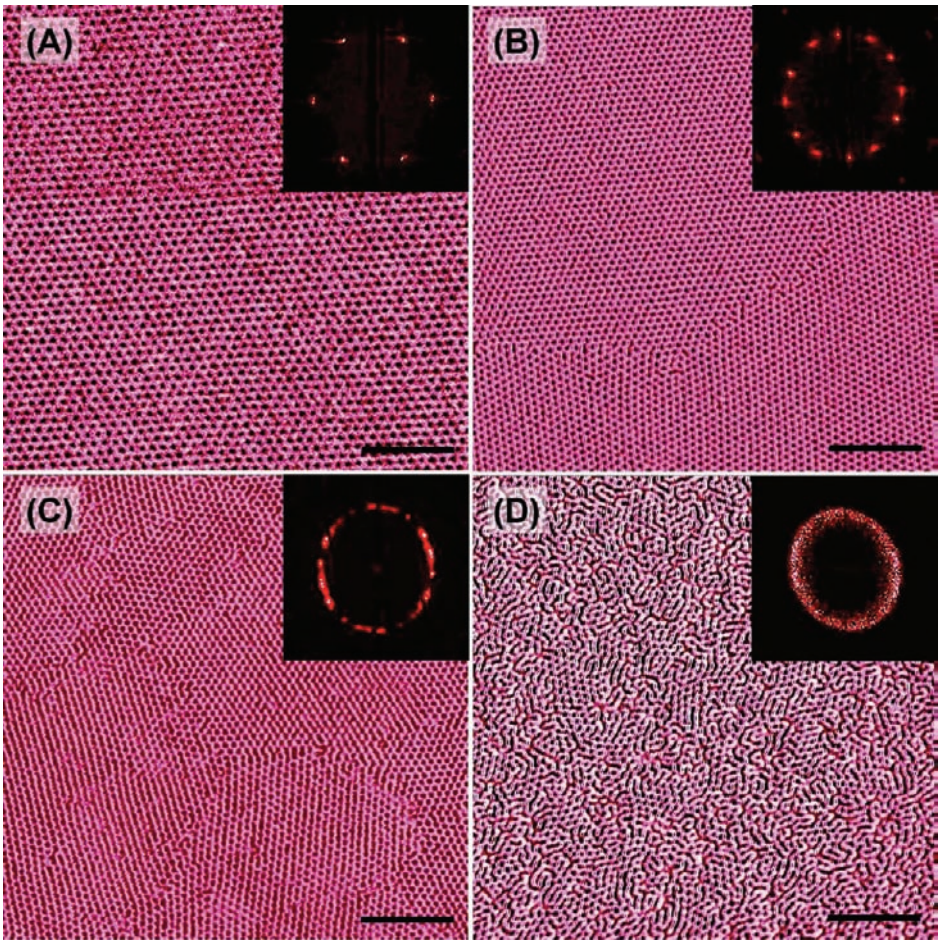

Figure 2. TMAFM phase images of PS-*b*-PB diblock copolymers prepared by zone casting with different substrate withdrawal speeds. (A) 2 μm/s; (B) 6 μm/s; (C) 102 μm/s; (D) 500 μm/s. Corresponding thickness of each film: (A) ~2200 nm; (B) ~1600 nm; (C) ~400 nm; (D) ~150 nm. Scale bar: 400 nm.

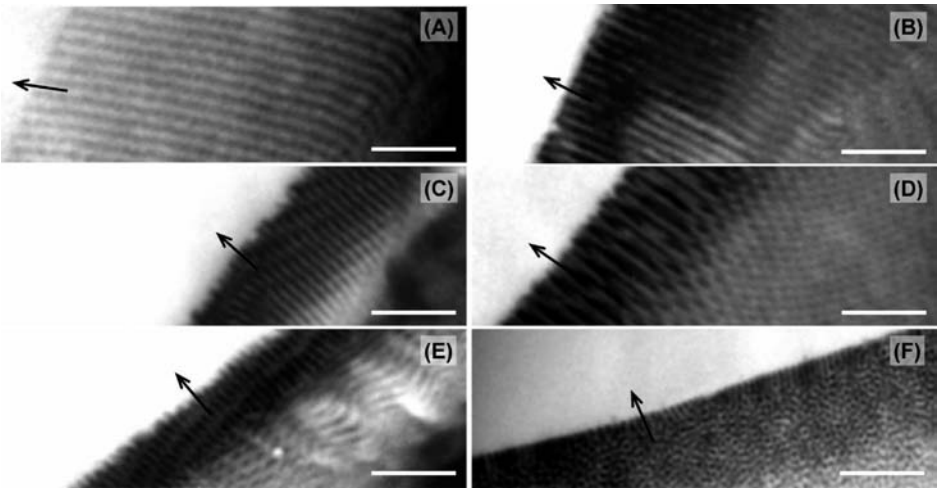

Figure 3. Cross-sectional TEM images of PS-*b*-PB samples prepared by zone casting at various substrate withdrawal speeds: (A) 2 μm/s; (B) 6 μm/s; (C) 18 μm/s; (D) 30 μm/s; (E) 54 μm/s; (F) 102 μm/s. Corresponding thickness of each film: (A) ~2200 nm; (B) ~1600 nm; (C) ~1000 nm; (D) ~800 nm; (E) ~600 nm; (F) ~400 nm. Arrows point to the film free surface. Scale bar: 200 nm.

withdrawal rate. One would expect that the withdrawal speed close to zero would result in the size of grains much larger than 10 μm and cylinders extending much deeper toward the substrate.

We also found that the PB cylinders were oriented parallel to some substrates (e.g., carbon-coated mica) in the immediate vicinity of the substrates. These results suggested the presence of

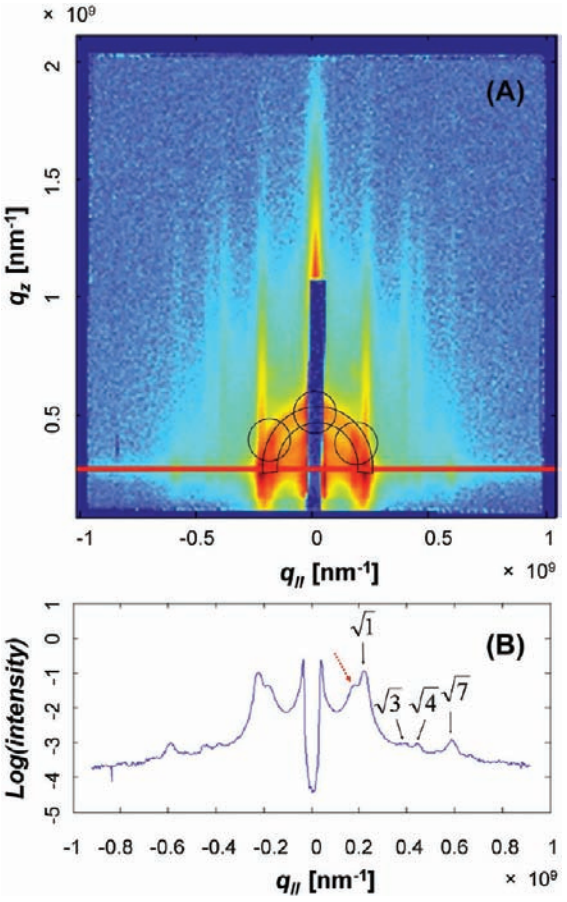

Figure 4. GISAXS of thin films of PS-*b*-PB block copolymers prepared by zone casting with substrate withdrawal speed at 18 μm/s: (A) GISAXS 2-D pattern acquired at 75° to casting direction at incidence angle 0.15; (B) corresponding GISAXS profile. The arrow pointed a peak at $q_{//}$ = 0.178.

strong anisotropy of the growth rate of hexagonally packed cylinders at the side of the film−air surface. The ordered grains grew faster in the longitudinal direction away from the film−air surface, given the fact that, at the low substrate withdrawal rate, cylinders oriented normal to the surface can effectively "outcompete" the domains with cylinders lying parallel to the substrate.

AFM and TEM techniques were successfully used to characterize the local structures of block copolymer thin films on the scale of up to tens of micrometers. To obtain a macroscopic understanding of thin films, we utilized grazing incidence small-angle X-ray scattering (GISAXS) to investigate both the top surface and internal structures of the thin films.[3,36,37,55−61] As can be seen from the GISAXS pattern acquired at 75° to the casting direction (Figure 4A), the block copolymer film produced at least 4 streak-like scattering rods (offset in $q_{//}$ and along the q_Z direction), whose relative scattering vector lengths (Figure 4B) were $\sqrt{1}$, $\sqrt{3}$, $\sqrt{4}$, and $\sqrt{7}$, respectively. The periodic spacing corresponding to the first maximum of Bragg rod was about 31 nm ($q_{//}$ = 0.20 nm^{-1}), very close to those obtained from AFM measurements. The scattering pattern with the spacing and orientation was consistent with hexagonally packed cylinders normal to the surface. We should point out that, below the first maximum of Bragg rod, there was ring-like scattering in the GISAXS 2-D pattern with an additional scattering peak next to the first maximum of hexagonal structures in the GISAXS profile, indicating the coexistence of another type of microdomains with a larger spacing about 35 nm ($q_{//}$ = 0.178) underneath the hexagonally packed cylinders. These observations agreed well with the TEM results. As mentioned above, cylinders normal to the film surface extended only to a certain depth. Below this depth, the cylinders were arranged randomly with respect to the surface.

The random orientation of cylinders produced ring-like features in the GISAXS 2D pattern (Figure 4A).[62] As the incident angle was above the critical angle of the substrate, both the direct beam and the reflected beam produced ring-like scattering, the offset of which was given by the incident angle. Note that there were blobs of enhanced intensity on the rings (the artificial rings in Figure 4A). These blobs can be identified as due to ordered cylinders, where the first cylinder layers formed parallel to the substrate. Other cylindrical domains, which were not correlated with the substrate surface and may have nucleated randomly above the first cylinder layers, produced the remaining ring intensity. Note that essentially only the first-order ring observed was indicative of short-range order in the parallel cylinders formed closer to the substrate.

Since the cylinders perpendicular to the surface did not extend to the full thickness of the films, one can use GISAXS to investigate the internal structures by changing the incidence angle, providing details on the depth dependence of the thin film structures and therefore influencing the GISAXS patterns. A series of incident angles ranging from 0.1 to 0.4 (the critical angle, α_c, was measured to be 0.127 for this block copolymer film) were used to control penetration depths from a few nanometers to full penetration of the entire films (Figure 5A). Below α_c (for example, 0.1), the peak at $q_{//}$ = 0.178 corresponding to randomly oriented cylinders was not observed in the GISAXS profile. It was probably because the X-ray penetration depth was smaller than the depth of cylinders normal to the surface and X-ray scattering was primarily contributed from the perpendicular cylinders in the near-surface region. However, above α_c (for example, 0.15, 0.175, 0.2, 0.3, 0.4), the peak at $q_{//}$ = 0.178 was clearly observed in all GISAXS profiles, and the higher the incidence angle, the stronger the peak, indicating the coexistence of cylinders perpendicular to the surface and cylinders parallel to the substrate.

The degree of orientation of perpendicular cylinders with respect to the casting direction was further investigated by acquiring GISAXS patterns at different azimuthal angles. Thin film samples were initially placed with the X-ray beam perpendicular to the casting direction and then rotated to certain angles. The scattering profiles of thin films at different azimuthal angles are shown in Figure 5B. All GISAXS patterns (not shown) and profiles appeared to be almost identical, indicating no preferred lateral orientation along the surface. This was further confirmed by continuously TMAFM imaging over tens of micrometers parallel to and perpendicular to the casting direction (Figure S1). Hence, the concentration gradient of polymer solution along the solidification front was not strong enough to orient the perpendicular cylinders with respect to the casting direction, as opposed to the situation found earlier for perpendicular lamellae of PAN-*b*-P*n*BA block copolymers, which were aligned perpendicular to the substrate withdrawal direction.[55]

Thin Films of Lamellar Block Copolymers by Zone-Casting. From the lithography point of view, zone casting of cylindrical PS-*b*-PB block copolymers was very striking, given potential

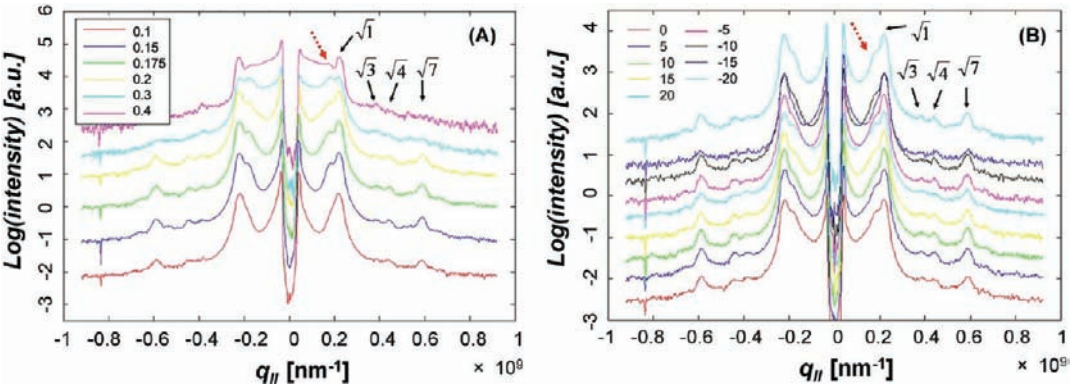

Figure 5. GISAXS profiles of thin films of PS-*b*-PB block copolymers prepared by zone casting with the substrate withdrawal speed at 18 μm/s: (A) incidence angle dependence of GISAXS profiles acquired at an azimuthal angle 5°; (B) azimuthal angle dependence of GISAXS profiles acquired at an incidence angle 0.15. The arrow pointed a peak at $q_{//} = 0.178$.

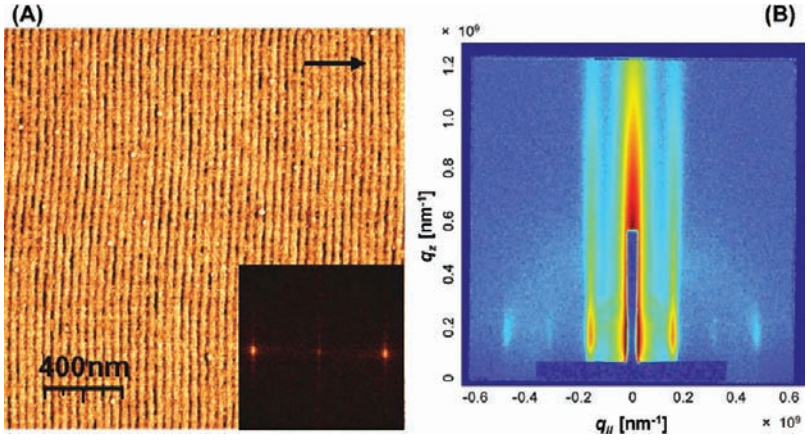

Figure 6. (A) TMAFM phase image (inset: FT transform), and (B) GISAXS pattern of PODMA-*b*-P*t*BA-*b*-PODMA block copolymer films prepared by zone casting at 40 °C. Arrow: substrate withdrawal direction.

degradability of PB cylinders (e.g., by ozonolysis) toward nanoporous lithographic resists. The orientation of a noncrystalline lamellar block copolymer by zone casting in our early work[55] was more consistent with other block copolymers induced by different strategies. We further extended zone casting[55] to a block copolymer containing a semicrystalline segment. The results herein can facilitate to better understand the mechanism of the zone casting process. Scheme 1B shows the zone casting process for a lamellar ABA triblock copolymer poly(octadecyl methacrylate)-*b*-poly(*t*-butyl acrylate)-*b*-poly(octadecyl methacrylate) (PODMA-*b*-P*t*BA-*b*-PODMA), which comprises a semicrystalline PODMA (melting point $T_m \approx 30$ °C) as the A block and an amorphous P*t*BA as the B block. The PODMA polymer is one of the polymers with an atactic main chain and crystallizable side chains.[63,64] The sample solution was deposited on a silicon wafer with a native oxide layer through zone casting from a concentration of 10 mg/mL in chloroform with the substrate withdrawal rate at 10 μm/s. The casting temperature was set at 40 °C, above the melting point of PODMA block. The film thickness was ~1200 nm. The lamellae with a periodicity of 41 nm were found to be consistently perpendicular to the surface. In the lateral plane, as shown in Figure 6A, the TMAFM phase image revealed that the lamellar orientation was perpendicular to the substrate withdrawal direction and extended at least hundreds of micrometer range, similar to our earlier work.[55]

Figure 6B showed the GISAXS pattern of the sample acquired with the X-ray beam at an angle of $\phi_0 = 90°$ with respect to the casting direction. The 2-D pattern further confirmed that the lamellae were perpendicular to both the substrate and the casting direction, which was again consistent with our earlier results on noncrystalline PAN-*b*-P*n*BA block copolymers.[55] The periodicity determined from the GISAXS pattern was equal to 40.7 nm. The results from GISAXS shown above were in good agreement with the TMAFM analysis. The second and third scattering peaks were also clearly visible from the pattern.

The degree of orientation was characterized by acquiring GISAXS patterns with the incident beam with respect to the casting direction $\phi = \phi_0 \pm 20°$. Partial azimuthal profiles of the scattering maximum were shown in Figure 7. The line shape of the azimuthal profiles obtained by GISAXS was better fitted by the Gaussian, instead of Lorentzian. The scattering intensity dropped to ~30% of the maximum value at an azimuthal angle of 0°. The half width at half height was found to be $\Delta\phi = 15°$, which indicated that the axis of the in-plane microdomain orientation fluctuated by ±15° in the macroscopic scale determined by GISAXS.

The noncrystallizable PODMA-*b*-P*t*BA-*b*-PODMA block copolymer film prepared by zone casting at 40 °C above the T_m of PODMA (crystallization of PODMA suppressed) resulted in the

lamellar orientation perpendicular to the casting direction, suggesting that the orientation was governed the microphase separation along the solidification front, which is always perpendicular to the casting direction. The imperfection of lateral orientation may be related with so-called "Mullins-Sekerka" instability, although it is originally used to explain metal alloy dentritic growth from initially flat surface.[65] We suspect that controlled solidification advancement in zone casting, when carried out at the "right" velocity, may stabilize the front against dendritic instability. On the other hand, zone casting process involves the transport of solute to the solidification line with evaporation of solvent, while the Mullins-Sekerka theory assumes no convection and usually large thermal gradients (e.g., metal alloy solidification).

Zone casting technique was originally designed to direct the growth of crystals of small molecules such as hexabenzocoronene.[47,53,54] Small molecules were found to self-assemble naturally toward the solidification front and the crystal columns were found to grow parallel to the substrate and the casting direction. To testify the above hypothesis for the orientation of noncrystallizable PODMA-*b*-P*t*BA-*b*-PODMA block copolymer films (as well as the noncrystalline PAN-*b*-P*n*BA block copolymers reported earlier), we prepared films of PODMA-*b*-P*t*BA-*b*-PODMA block copolymers by zone casting at a temperature of 20 °C, which was below the T_m of the PODMA block. Our earlier work indicated that the crystallization should occur during the evaporation process of solvent.[63,64] While the order of lamellar structures perpendicular to the substrate was well maintained (Figure 8A), the lamellae were found to be parallel to the casting direction, similar to the orientation of those molecular crystals reported earlier.[47,53,54] The periodicity determined from the GISAXS pattern (Figure 8B) was equal to 44.5 nm, which was in good agreement with the one (43.2 nm) determined by the 2-D Fourier transform (FT) of AFM image (Figure 8A). However, the periodicity was somewhat nearly 10% larger than the films cast above the T_m of PODMA. Azimuthal angle studies indicated that the global ordering of block copolymer films cast above the melting temperature of PODMA was similar to the films cast below the melting temperature of PODMA (Figure 7). An illustration of such orientation is shown in Figure 8C.

Strikingly, the above lamellar orientation was observed in various substrates like those used for zone casting of cylindrical PS-*b*-PB block copolymers, indicating that the ordering nucleated from the surface and propagated toward the substrates.

The above results indicated that the orientation of the lamellae of semicrystalline block copolymers is greatly dependent on the casting conditions, particularly the casting temperature. When the zone casting was employed below the melting temperature of PODMA block, the crystallization of PODMA occurred when the block copolymer solidified at the solid−liquid interface (the solidification front). The PODMA lamellae kept advancing along the concentration gradient of polymer solution (perpendicular to the solidification front), remarkably similar to the crystallization-driven orientation of molecular crystals in the zone casting observed earlier,[47,53,54] while the amorphous P*t*BA domain was forced to solidify along the PODMA domains. Above the melting temperature of PODMA (therefore no crystallization, the block copolymers behaved like amorphous polymers), the orientation of lamellae perpendicular to the casting direction in films prepared by zone casting was governed by their attempt to microphase-separate along the solidification front (solid−liquid interface) (slowly advancing with the withdrawal of substrate) rather than to advance along the concentration gradient of polymer solution. The PODMA and P*t*BA segments have different diffusion rates at the interface of solid and solution, thus, leading to the solidification of one domain followed by the other alternatively. This was also consistent with the orientation of

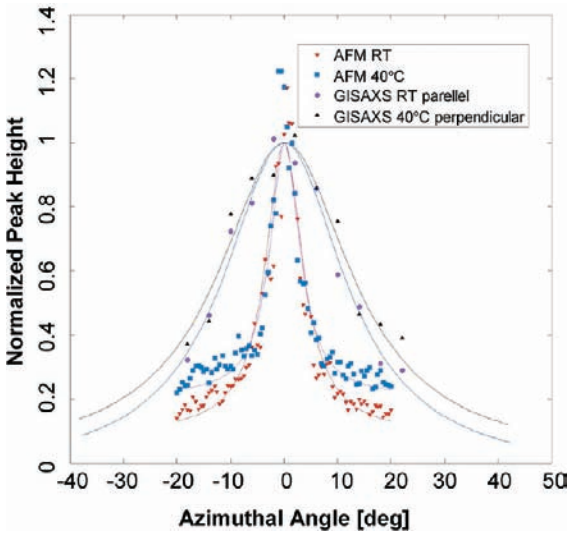

Figure 7. Azimuthal profiles of maxima in 2-D Fourier transforms of AFM images and maxima in GISAXS patterns corresponding to the lamellar period.

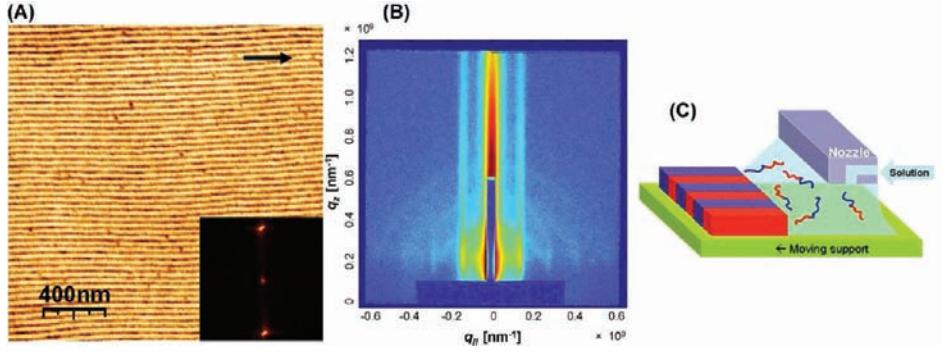

Figure 8. (A) TMAFM phase image (inset: FT transform), (B) GISAXS pattern of PODMA-*b*-P*t*BA-*b*-PODMA block copolymer films prepared by zone casting at 20 °C, and (C) an illustration of zone-casting of crystallizable block copolymers with a lamellar morphology. Arrow: substrate withdrawal direction.

dx.doi.org/10.1021/ja204724h |*J. Am. Chem. Soc.* 2011, 133, 11802–11809

noncrystalline diblock copolymer PAN-*b*-P*n*BA, where the lamellae of PAN-*b*-P*n*BA were also found to be perpendicular to the casting direction.[55]

In conclusion, a robust zone casting technique has been developed to prepare highly ordered thin films of block copolymers with versatile nanostructures. Both cylinders and lamellae exhibited striking orientational order, perpendicular to the film surface, while the lateral order depended on the block copolymer chemistry and casting conditions. For block copolymers with a cylindrical morphology, the size of ordered gains and the penetration depth of cylinders perpendicular to the surface increased with the decrease of the substrate withdrawal rate. The domain orientation seemed to be irrelevant with the casting direction. For block copolymers with a lamellar morphology, the lamellar orientation with respect to the casting direction is classified into two different situations: (1) For noncrystallizable block copolymers, the lamellar orientation is perpendicular to the casting direction, (2) while lamellae in the crystallizable block copolymers adopt parallel orientation to the casting direction. The overall orientation of lamellae is governed by the competition between the microphase separation along the solidification front (solid−liquid interface) and the crystallization along the concentration gradient perpendicular to the solidification front. This fundamental understanding on the block copolymer orientation paves the way to potentially allow a variety of block copolymers to obtain highly ordered thin films, which are critical for many useful applications.

EXPERIMENTAL SECTION

Materials. A triblock copolymer PODMA-*b*-p*t*BA-*b*-PODMA (structure formula: $ODMA_{58}tBA_{437}ODMA_{58}$) was synthesized by Atom Transfer Radical Polymerization (ATRP).[66−68] Difunctional bromo-terminated Br-P(*t*-butyl acrylate)-Br was first synthesized through ATRP, followed by a chain extension with the PODMA block using halogen exchange with CuCl as the catalyst,[67] yielding a block copolymer ($ODMA_{58}tBA_{437}ODMA_{58}$, M_n = 94 900 and M_w/M_n = 1.18, with 41.0 wt % ODMA). A cylindrical diblock copolymer polystyrene-*b*-poly(1,4-butadiene) (PS-*b*-PB) is composed of 32 wt.% PB and has a PDI of 1.03 (structure formula: $S_{273}B_{323}$, Polymer Source, Inc.).

Film Preparation by Zone Casting. Zone casting was performed using a home-built apparatus, equipped with two computer-controlled linear stages and independently controlled solution and substrate temperature controllers. Diblock copolymer PS-*b*-PB was dissolved in chloroform with a 10 mg/mL concentration. This particular copolymer forms a cylindrical morphology, in which PB cylinders are dispersed in a PS matrix. Zone casting was performed under ambient conditions by depositing the copolymer solution onto a moving substrate with the aid of a syringe equipped with a flat nozzle, which is about or less than 1.0 mm above the moving substrate (Scheme 1). The substrate was withdrawn at different speeds (e.g., 2, 6, 18, 30, 54, 102, and 256 μm/s) with the syringe plunger displaced at a nearly constant speed (~14 μm/s) using two separate computer-controlled stepper motors. Zone casting of triblock copolymer PODMA-*b*-p*t*BA-*b*-PODMA solution was similar. The polymer was dissolved in chloroform with a concentration of 10 mg/mL. The supply rate of the solution was 10 μm/s and the moving speed of the substrate was 11 μm/s. When the casting was carried out above the T_m (~30 °C) of PODMA, both the substrate temperature and the solution temperature were maintained at 40 °C, while below T_m, the temperatures of the substrate and the solution were adjusted to 20 °C.

Atomic Force Microscopy. TMAFM experiments were carried out using a Multimode Nanoscope III system (Digital Instruments, Santa Barbara, CA). The measurements were performed under ambient atmosphere using commercial Si cantilevers with a spring constant and resonance frequency respectively equal to 21−78 N/m and 250−390 kHz. The height and phase images were acquired simultaneously at the set-point ratio A/A_o = 0.7, where A and A_o refer, respectively, to the "tapping" and "free" cantilever amplitude.

Grazing Incidence Small Angle X-ray Scattering (GISAXS). GISAXS images were taken at CHESS D station (Cornell University). A wide bandpass (1.7%) double-bounce multilayer monochromator supplied an intense beam of 10 keV photons which impinged onto the sample surface under various incident angles ranging from below the critical angle of the film and above the critical angle of the substrate. The sample was mounted on a sample goniometer, in order to control the incident angle and the sample azimuth. An accurate calibration of the incident angle was performed in situ by measuring the X-ray reflectivity from the sample using an ion chamber. GISAXS scattering intensities were recorded with an area detector (Medoptics) with a resolution of 50 μm/pixel and a total area of about 50 mm × 50 mm at a distance of 1280 mm from the sample. Exposure time under these conditions ranged from 1 to 30 s depending on contrast and sample quality.

Transmission Electron Microscopy (TEM). TEM images were obtained by staining the films overnight with OsO_4. The films were embedded in Epon-Araldite resin and cured at 60 °C. The embedded films were then microtomed at room temperature and examined with a Hitachi H-7100 electron microscope operating at 70 kV.

ASSOCIATED CONTENT

Supporting Information. Overlayed TMAFM phase images of PS-*b*-PB diblock copolymers prepared by zone casting (Figures S1−S3) and grain size vs casting speed (Figure S4). This material is available free of charge via the Internet at http://pubs.acs.org.

AUTHOR INFORMATION

Corresponding Author
tomek@andrew.cmu.edu; km3b@andrew.cmu.edu; tang.c@chem.sc.edu

ACKNOWLEDGMENT

We gratefully thank Prof. Edward J. Kramer for helpful discussions. This work has been supported by National Science Foundation (NIRT 0210247 and DMR 0090409). Support from University of South Carolina (Start-up fund, C.T.) is acknowledged. CHESS is supported by the NSF and NIH/NIGMS via NSF award DMR-0936384.

REFERENCES

(1) Whitesides, G. M.; Grzybowski, B. *Science* **2002**, *295*, 2418–2422.
(2) Gracias, D.; Tien, J.; Breen, T. L.; Hsu, C.; Whitesides, G. M. *Science* **2000**, *289*, 1170.
(3) Ozin, G. A.; Hou, K.; Lotsch, B. V.; Cademartiri, L.; Puzzo, D. P.; Scotognella, F.; Ghadimi, A.; Thomson, J. *Mater. Today* **2009**, *12*, 12–23.
(4) Bates, F. S.; Fredrickson, G. H. *Phys. Today* **1999**, *52*, 32–38.
(5) Bates, F. S.; Fredrickson, G. H. *Annu. Rev. Phys. Chem.* **1990**, *41*, 525–557.
(6) Fredrickson, G. H.; Bates, F. S. *Annu. Rev. Mater. Sci.* **1996**, *26*, 501–550.
(7) Hadjichristidis, N.; Pispas, S.; Floudas, G. *Block Copolymers: Synthetic Strategies, Physical Properties, and Applications*; John Wiley & Sons, Inc.: Hoboken, NJ, 2003.
(8) Hamley, I. W. *The Physics of Block Copolymers*; Oxford University Press: Oxford, U.K., 1998.

(9) Lazzari, M.; Lopez-Quintela, M. A. *Adv. Mater.* **2003**, *15*, 1583–1594.
(10) Fasolka, M. J.; Mayes, A. M. *Annu. Rev. Mater. Res.* **2001**, *31*, 323–355.
(11) Hamley, I. W. *Prog. Polym. Sci.* **2009**, *34*, 1161–1210.
(12) Kim, J. K.; Yang, S. Y.; Lee, Y.; Kim, Y. *Prog. Polym. Sci.* **2010**, *35*, 1325–1349.
(13) Larisa, T.; Agur, S. G. J.; Georg, K. *Adv. Polym. Sci.* **2010**, *227*, 33–73.
(14) Ho-Cheol, K.; Sang-Min, P.; Hinsberg, W. D. *Chem. Rev.* **2010**, *110*, 146–177.
(15) Albert, J. N. L.; Epps, T. H., III. *Mater. Today* **2010**, *13*, 24–33.
(16) Park, M.; Harrison, C.; Chaikin, P. M.; Register, R. A.; Adamson, D. H. *Science* **1997**, *276*, 1401–1404.
(17) Kim, S. O.; Solak, H. H.; Stoykovich, M. P.; Ferrier, N. J.; de Pablo, J. J.; Nealey, P. F. *Nature* **2003**, *424*, 411–414.
(18) Ross, C. *Annu. Rev. Mater. Res.* **2001**, *31*, 203–235.
(19) Hillmyer, M. A. *Adv. Polym. Sci.* **2005**, *190*, 137–181.
(20) Cheng, J. Y.; Ross, C. A.; Smith, H. I.; Thomas, E. L. *Adv. Mater.* **2006**, *18*, 2505–2521.
(21) Segalman, R. A. *Mater. Sci. Eng., R* **2005**, *R48*, 191–226.
(22) Bang, J.; Jeong, U.; Ryu, D. Y.; Russell, T. P.; Hawker, C. J. *Adv. Mater.* **2009**, *21*, 4769–4792.
(23) Park, C.; De Rosa, C.; Lotz, B.; Fetters, L. J.; Thomas, E. L. *Macromol. Chem. Phys.* **2003**, *204*, 1514–1523.
(24) Mansky, P.; Liu, Y.; Huang, E.; Russell, T. P.; Hawker, C. J. *Science* **1997**, *275*, 1458–1460.
(25) Ryu, D. Y.; Shin, K.; Drockenmuller, E.; Hawker, C. J.; Russell, T. P. *Science* **2005**, *308*, 236–239.
(26) Amundson, K.; Helfand, E.; Davis, D. D.; Quan, E.; Patel, S. S.; Smith, S. D. *Macromolecules* **1991**, *24*, 6546–6548.
(27) Amundson, K.; Helfand, E.; Quan, E.; Hudson, S. D.; Smith, S. D. *Macromolecules* **1994**, *27*, 6559–6570.
(28) Mansky, P.; DeRouchey, J.; Russell, T. P.; Mays, J.; Pitsikalis, M.; Morkved, T.; Jaeger, H. *Macromolecules* **1998**, *31*, 4399–4401.
(29) Morkved, T. L.; Lu, M.; Urbas, A. M.; Ehrichs, E. E.; Jaeger, H. M.; Mansky, P.; Russell, T. P. *Science* **1996**, *273*, 931–933.
(30) Schmidt, K.; Schoberth, H. G.; Ruppel, M.; H., Z.; Hänsel, H.; Weiss, T. M.; Urban, V.; Krausch, G.; Böker, A. *Nat. Mater.* **2008**, *7*, 142–145.
(31) Gopinadhan, M.; Majewski, P. W.; Osuji, C. O. *Macromolecules* **2010**, *43*, 3286–3293.
(32) Albalak, R. J.; Thomas, E. L. *J. Polym. Sci., Part B: Polym. Phys.* **1994**, *32*, 341–350.
(33) Segalman, R. A.; Hexemer, A.; Kramer, E. J. *Macromolecules* **2003**, *36*, 6831–6839.
(34) Segalman, R. A.; Hexemer, A.; Kramer, E. J. *Phys. Rev. Lett.* **2003**, *91*, 196101–196104.
(35) Segalman, R. A.; Yokoyama, H.; Kramer, E. J. *Adv. Mater.* **2001**, *13*, 1152–1155.
(36) Stein, G. E.; Kramer, E. J.; Li, X.; Wang, J. *Phys. Rev. Lett.* **2007**, *98*, 086101.
(37) Stein, G. E.; Kramer, E. J.; Li, X.; Wang, J. *Macromolecules* **2007**, *40*, 2453–2460.
(38) Bita, I.; Yang, J. K. W.; Ross, C. A.; Thomas, E. L.; Berggren, K. K. *Science* **2008**, *321*, 939–943.
(39) Park, S.; Lee, D. H.; Xu, J.; Kim, B.; Hong, S. W.; Jeong, U.; Xu, T.; Russell, T. P. *Science* **2009**, *323*, 1030–1033.
(40) Ruiz, R.; Kang, H.; Detcheverry, F. A.; Dobisz, E.; Kercher, D. S.; Albrecher, T. R.; de Pable, J. J.; Nealey, P. F. *Science* **2008**, *321*, 936–939.
(41) De Rosa, C.; Park, C.; Thomas, E. L.; Lotz, B. *Nature* **2000**, *405*, 433–437.
(42) Reiter, G.; Castelein, G.; Hoerner, P.; Riess, G.; Blumen, A.; Sommer, J. U. *Phys. Rev. Lett.* **1999**, *83*, 3844–3847.
(43) Kim, S. H.; Misner, M. J.; Russell, T. P. *Adv. Mater.* **2004**, *16*, 2119–2123.
(44) Kim, S. H.; Misner, M. J.; Xu, T.; Kimura, M.; Russell, T. P. *Adv. Mater.* **2004**, *16*, 226–231.
(45) Bang, J.; Kim, B. J.; Stein, G. E.; Russell, T. P.; Kramer, E. J.; Hawker, C. J. *Macromolecules* **2007**, *40*, 7019–7025.
(46) Bang, J.; Kim, S. H.; Drockenmuller, E.; Misner, M. J.; Russell, T. P.; Hawker, C. J. *J. Am. Chem. Soc.* **2006**, *128*, 7622–7629.
(47) Breiby, D. W.; Bunk, O.; Pisula, W.; Sølling, T. I.; Tracz, A.; Pakula, T.; Müllen, K.; Nielsen, M. M. *J. Am. Chem. Soc.* **2005**, *127*, 11288–11293.
(48) Tang, C.; Bang, J.; Stein, G. E.; Fredrickson, G. H.; Hawker, C. J.; Kramer, E. J.; Sprung, M.; Wang, J. *Macromolecules* **2008**, *41*, 4328–4339.
(49) Tang, C.; Hur, S.; Stahl, B. C.; Sivanandan, K.; Dimitriou, M.; Pressly, E.; Fredrickson, G. H.; Kramer, E. J.; Hawker, C. J. *Macromolecules* **2010**, *43*, 2880–2889.
(50) Tang, C.; Lennon, E. M.; Fredrickson, G. H.; Kramer, E. J.; Hawker, C. J. *Science* **2008**, *322*, 429–432.
(51) Tang, C.; Sivanandan, K.; Brian, C. S.; Fredrickson, G. H.; Kramer, E. J.; Hawker, C. J. *ACS Nano* **2010**, *4*, 285–291.
(52) Kimura, M.; Misner, M. J.; Xu, T.; Kim, S. H.; Russell, T. P. *Langmuir* **2003**, *19*, 9910–9913.
(53) Pisula, W.; Menon, A.; Stepputat, M.; Lieberwirth, I.; Kolb, U.; Tracz, A.; Sirringhaus, H.; Pakula, T.; Mullen, K. *Adv. Mater.* **2005**, *17*, 684–689.
(54) Tracz, A.; Jeszka, J. K.; Watson, M. D.; Pisula, W.; Mullen, K.; Pakula, T. *J. Am. Chem. Soc.* **2003**, *125*, 1682–1683.
(55) Tang, C.; Tracz, A.; Kruk, M.; Zhang, R.; Smilgies, D.-M.; Matyjaszewski, K.; Kowalewski, T. *J. Am. Chem. Soc.* **2005**, *127*, 6918–6919.
(56) Smilgies Detlef, M.; Busch, P.; Posselt, D.; Papadakis, C. M. *Synchrotron Radiat. News* **2002**, 35–41.
(57) Lee, B.; Park, I.; Yoon, J.; Park, S.; Kim, J.; Kim, K. W.; Chang, T.; Ree, M. *Macromolecules* **2005**, *38*, 4311–4323.
(58) Lee, B.; Yoon, J.; Oh, W.; Hwang, Y.; Heo, K.; Jin, K. S.; Kim, J.; Kim, K. W.; Ree, M. *Macromolecules* **2005**, *38*, 3395–3405.
(59) Muller-Buschbaum, P. *Anal. Bioanal. Chem.* **2003**, *376*, 3–10.
(60) Muller-Buschbaum, P.; Roth, S. V.; Burghammer, M.; Bauer, E.; Pfister, S.; David, C.; Riekel, C. *Physica B* **2005**, *357*, 148–151.
(61) Muller-Buschbaum, P.; Wunnicke, O.; Stamm, M.; Lin, Y. C.; Muller, M. *Macromolecules* **2005**, *38*, 3406–3413.
(62) Lee, B.; Oh, W.; Hwang, Y.; Park, Y. H.; Yoon, J.; Jin, K. S.; Heo, K.; Kim, J.; Kim, K. W.; Ree, M. *Adv. Mater.* **2005**, *17*, 696–701.
(63) Wu, W.; Matyjaszewski, K.; Kowalewski, T. *Langmuir* **2005**, *21*, 1143–1148.
(64) Wu, W.; Huang, J.; Jia, S.; Kowalewski, T.; Matyjaszewski, K.; Pakula, T.; Gitsas, A.; Floudas, G. *Langmuir* **2005**, *21*, 9721–9727.
(65) Mullins, W. W.; Sekerka, R. F. *J. Appl. Phys.* **1964**, *35*, 444–450.
(66) Matyjaszewski, K.; Xia, J. *Chem. Rev.* **2001**, *101*, 2921.
(67) Qin, S. H.; Saget, J.; Pyun, J. R.; Jia, S. J.; Kowalewski, T.; Matyjaszewski, K. *Macromolecules* **2003**, *36*, 8969–8977.
(68) Wang, J. S.; Matyjaszewski, K. *J. Am. Chem. Soc.* **1995**, *117*, 5614–5615.